

UC Davis

UC Davis Previously Published Works

Title

“Ready-to-use” immunosensor for the detection of small molecules with fast readout

Permalink

<https://escholarship.org/uc/item/1f0102nr>

Authors

Ding, Yuan
Cui, Panpan
Chen, He
et al.

Publication Date

2022-04-01

DOI

10.1016/j.bios.2022.113968

Peer reviewed



HHS Public Access

Author manuscript

Biosens Bioelectron. Author manuscript; available in PMC 2023 April 01.

Published in final edited form as:

Biosens Bioelectron. 2022 April 01; 201: 113968. doi:10.1016/j.bios.2022.113968.

“Ready-to-use” immunosensor for the detection of small molecules with fast readout

Yuan Ding^{a,b}, Panpan Cui^{a,b}, He Chen^{a,b}, Jiao Li^{a,b}, Lianrun Huang^{a,b}, Gualberto González-Sapienza^d, Bruce D. Hammock^c, Minghua Wang^{a,b}, Xiude Hua^{a,b,*}

^aCollege of Plant Protection, Nanjing Agricultural University, Nanjing 210095, China

^bState & Local Joint Engineering Research Center of Green Pesticide Invention and Application, Nanjing 210095, China

^cDepartment of Entomology and UCD Cancer Center, University of California, Davis, CA 95616, United States

^dCátedra de Inmunología, Facultad de Química, Instituto de Higiene, Universidad de la República, Montevideo 11600, Uruguay

Abstract

Immunoassays are commonly used methods for detection of small molecules that typically require numerous steps of the labeling between immune-recognition reagents and tracers, immobilization and recurrent washing, making them time consuming and difficult to adapt into point of care formats. Here we describe a “ready-to-use” homogeneous competitive immunosensor with an assay time of 10 min that is based exclusively on recombinant reagents. The signal is produced when the split fragments of the nano luciferase (Nluc) are brought together by the interaction of a heavy chain only variable domain (VHH) with a peptidomimetic of the target small molecule. A VHH to 2,4-dichlorophenoxyacetic acid (2,4-D) was used to isolate the peptidomimetic (NGFFEPWQVVYV) from phage display libraries using six panning conditions. Then the peptidomimetic and VHH were fused with the larger (LgN) and smaller piece (SmN) of split fragments of Nluc, respectively. In order to optimize the signal and sensitivity of the immunosensor, we explored the effects of the spacer between the peptidomimetic and LgN, the copy number of peptidomimetics, and the spacer between SmN and VHH, generating 24 combinations that allowed to conclude on their respective roles. Eventually, the developed “ready-to-use” immunosensor performed excellent signal-to-noise ratio and sensitivity, and could be applied to the detection of 2,4-D in real samples. Meanwhile, the immunosensor totally realizes labeling-free, immobilization-free and washing-free, also can be produced in a highly cost effective way.

Keywords

Immunosensor; Label free; Peptidomimetic; Split luciferase; Small molecule

*Corresponding author. College of Plant Protection, Nanjing Agricultural University, Nanjing 210095, China, Tel.: +86 25 84395479. Fax: +86 25 84395479. huaxiude@njau.edu.cn (X.H. Hua).

1. Introduction

The COVID-19 pandemic has demonstrated the powerful role of rapid diagnostic capabilities in controlling the spread of disease. In the future, the demands for the detection reagents and test results, which can be produced and obtained quickly, are evident in broader diagnostic or testing applications (Adamson et al., 2020). Also, small molecular compounds, such as pesticides, toxins, organic pollutants and drugs, are usually related to the issues of food safety, environmental pollution and health care. So these small molecule targets reinforce the need for rapid detection capability, such rapid, quantitative analysis is of great significance to provide timely monitoring or warning (Wang et al., 2018). Among the rapid detection methods for small molecules, immunoassay utilizing specific binding of antibody and antigen has been widely recognized and used thanks to its advantages of general applicability, high sensitivity, simplicity and cheapness (Fang et al., 2020; Yao et al., 2020). Over the past four decades, immunoassays have been adapted to different tracer reagents and detection platforms resulting in a variety of immunoassay modes, such as enzyme-linked immunosorbent assay (ELISA) (Fang et al., 2020), lateral flow immunoassays (Wu et al., 2020), electrochemical immunosensors (Ai et al., 2021), and some homogeneous assays (Kang et al., 2020; Takkinen et al., 2019). However, a major drawback of current immunoassays is that the recognition and signal generation require independent reagents (Adamson et al., 2020). It makes the procedures of labeling, immobilization or washing unavoidable, which further increases the analysis time and the production cycle of test reagents. Besides, the labeling and redundant analysis steps also increase the batch-to-batch variation and analytical errors.

For the above considerations, we propose to merge the preparations of the two types reagents and make them respond to the input of analyte quickly, in a sensitive and reliable way, so that provides a ready-to-use and fast readout immunosensor for the detection of small molecules. Fusion expression by microorganisms was considered the appropriate way to integrate the two reagents, in which the recombinant bifunctional reagents can be produced on large-scale by microbial fermentation and have the fixed stoichiometric ratios between the recognition and signal generation reagents (Ding et al., 2018). However, this approach is somewhat awkward for the application to small molecule immunoassay. This is because the dominant immunoassay for small molecule is usually a competitive format that requires a chemical hapten to compete with the analyte for binding to the antibody (Yao et al., 2020). In recent years, some researchers utilized the peptidomimetics isolated from phage display libraries replacing chemical haptens, and fused them with protein tracers to develop the immunoassays (Ding et al., 2018; Luque-Uria et al., 2021; Peltomaa et al., 2020; Peltomaa et al., 2018). But some problems should be noticed, a) monoclonal antibodies were used in all these reports, despite the long time and high cost to produce monoclonal antibodies, there is still no actual avoidance of labeling or immobilization; b) the fusion processes usually reduce the peptidomimetic's valences that may result in an inability to generate detectable signals or too high background in usual immunoassay modes (Chen et al., 2019; Vanrell et al., 2013).

Heavy chain only variable domain (VHH) antibodies can be produced by biological expression. They also show high solubility and stability, and are good substitute for

monoclonal antibodies (Liu et al., 2021). In this work, we explored a “ready-to-use” immunosensor with fast readout using a pair of immunorecognition reagents that are seldom used, VHH and a peptidomimetic. A peptidomimetic (NGFFEPWQVVYV) recognizing an anti-2,4-dichlorophenoxyacetic acid (2,4-D) VHH (Li et al., 2021) (VHH_{2,4-D}) was isolated from phage display libraries using six panning conditions, and the conditions conducive to peptidomimetic acquisition were analyzed. Then, the VHH_{2,4-D} and peptidomimetic were fused with two split fragments of nano luciferase (Nluc), the smaller piece (SmN, 1.3 kDa) and the larger piece (LgN, 17.7 kDa), respectively. The recognition between VHH_{2,4-D} and peptidomimetic would promote the reassociation of LgN and SmN into functional Nluc and restore the luminescence in the system (Dixon et al., 2016). In order to achieve better performance, the roles of the spacer between peptidomimetic and LgN, the copy number of peptidomimetics and the spacer between SmN and VHH_{2,4-D} were analyzed in development of the “ready-to-use” immunosensor from two processes: the recognition between peptidomimetic and VHH_{2,4-D}, and the reassociation of LgN and SmN. Thus, the ready-to-use immunosensor with a high positive signal (luminescence intensity of the immunosensor when there is no 2,4-D), high signal-to-noise (S/N) ratio and high sensitivity was successfully developed and used for the detection of 2,4-D in both quantitative and visual ways.

2. Materials and methods

2.1. Materials

The materials and reagents used in this research are described in supplementary information (SI).

2.2. Protein preparation

The expression plasmid for MBP-VHH_{2,4-D} was pMAL-p5X that already carries the gene of MBP, and the gene of VHH_{2,4-D} was inserted between the cloning sites of *Not*I and *Eco*R I. The plasmid pET22b was employed to express VHH_{2,4-D} and other four VHH_{2,4-D}-derived proteins, including the recombinant proteins of VHH_{2,4-D} and SmN (SmN-VHHs) with no spacer (SmNVHH), spacer of -GGGSGGGS- (SmN-S₁-VHH), spacer of -(GGGSGGGS)₂- (SmN-S₂-VHH) and spacer of -(GGGSGGGS)₃- (SmN-S₃-VHH). The plasmid pET28a was employed to express LgN and the recombinant proteins of peptidomimetic and LgN (Pm-LgNs), including the recombinant proteins of monovalent peptidomimetic and LgN without spacer (PLgN) and with a spacer of -GGGSGGGS- (P-LgN) between the peptidomimetic and LgN, divalent peptidomimetic and LgN without spacer (P²LgN) and with a spacer of -GGGSGGGS- (P²-LgN), trivalent peptidomimetic and LgN without spacer (P³LgN) and with a spacer of -GGGSGGGS- (P³-LgN).

The *E. coli* strain BL21(DE3) was used to express above proteins, which were induced at 25 °C with 1mM IPTG for overnight. There is a pelB signal peptide on the plasmids pMAL-p5X and pET22b that can lead MBP-VHH_{2,4-D}, VHH_{2,4-D} and SmN-VHHs into the periplasm, so the “osmotic shock method” was applied to extract those proteins. Other proteins located in cytoplasm were extracted using a cell lysis solution. MBP-VHH_{2,4-D} was purified by amylose resin and then a Ni-NTA column. PLgN and P²LgN were purified

by Ni-NTA column and then size-exclusion chromatography. Other proteins were directly purified by Ni-NTA column.

2.3. Binding assays

Series of concentrations of SmN-VHHs were used to titrate Pm-LgNs. SmN-VHH, Pm-LgN and 1 μL Nluc substrate were mixed in PBS buffer (pH 7.4) containing 1 mg mL^{-1} bovine serum albumin (BSA) and incubated in the white microplate with nonbinding surface. Then the luminescence intensities (RLUs) were monitored with SpectraMax M5 every 6 s for 10 min. The observed rate constants (k_{obs}) at different concentrations of SmN-VHH were calculated by GraphPad Prism 8 using the one phase association equation (Dixon et al., 2016). The association (k_{on}) and dissociation (k_{off}) rates were determined by linear fitting the concentrations of SmN-VHHs and k_{obs} s according to the following formula:

$$k_{\text{obs}} = k_{\text{on}} \times [\text{SmN-VHH}] + k_{\text{off}}$$

2.4. Immunosensor detection

Seventy microliter mixtures of Pm-LgN and SmN-VHH in 1 mg mL^{-1} BSA-PBS were added to the white microplate with nonbinding surface. Then 20 μL 2,4-D standard solutions or sample solutions were injected and reacted under gentle shaking at room temperature. After the reaction, 10 μL of PBS containing 0.4 μL Nluc substrate was added to generate bioluminescence, which the RLUs can be measured by a SpectraMax M5 or observed by the naked eye in a black box.

The details for biopanning, plasmids construction and the primers (Table S1), amino acid sequences of the proteins used, phage ELISA, cross-reactivities and spiked sample analysis are described in SI.

3. Results and discussion

3.1. Peptidomimetic acquisition

The peptidomimetics have been reported extensively in monoclonal antibodies-based immunoassays, which can be easily obtained by several rounds of biopanning, and usually show better sensitivities than chemical haptens (Zhao et al., 2021). However, there is only one report on peptidomimetic that can recognize VHH (Zhao et al., 2019). In that research, the VHH was labelled with biotin through a fused Avi tag, and then was attached to streptavidin modified magnetic beads as the target receptor for biopanning procedure, which allowed to isolate several 12-amino-acid peptidomimetics. Whereas, we preferred to use the microplate for peptidomimetic biopanning, which is the more common approach that can avoid more labeling steps and reagent requirements. Given that peptidomimetics against monoclonal antibodies are relatively easy to obtain, and one of the biggest differences between VHH and monoclonal antibody is molecular weight, we prepared the recombinant protein of VHH_{2,4-D} and maltose-binding protein (MBP) (MBP-VHH_{2,4-D}) (Fig. 1a), and simultaneously used VHH_{2,4-D} and MBP-VHH_{2,4-D} as the target receptors to screen phage display 7-amino-acids, cyclic 7-amino-acids and 12-amino-acids random peptide libraries. Eventually, a phage display peptidomimetic (amino acid sequence: NGFFEPWQVVYV)

was obtained from the 12-amino-acids peptide library using MBP-VHH_{2,4-D} as the target receptor (Table S2).

To explain why no peptidomimetic was isolated using VHH_{2,4-D}, phage ELISAs were employed to measure the differences in reactivities of the phage display peptidomimetic and its sensitivities for the detection of 2,4-D using VHH_{2,4-D} and MBP-VHH_{2,4-D} as the target receptors, respectively. The results showed that the reactivity to MBP-VHH_{2,4-D} was much higher than to VHH_{2,4-D} under the same coated mass (Fig. 1b), and there was higher 50% inhibitory concentration (IC₅₀) when used VHH_{2,4-D} as target receptor, even part of bound phages cannot be dissociated by 2,4-D (Fig. 1c). At first, we suspected that the less hydrophobic regions or ionic groups on the smaller VHH_{2,4-D} caused the mild adsorption by microplate so that the coated VHH_{2,4-D} shed in ELISA procedures, which resulted in the decrease of actual coated mass and the increased in nonspecific binding of the phages to the blank sites. In order to check this suspicion, series of concentrations of VHH_{2,4-D} were coated on the microplates, then HRP-labelled anti-VHH antibody was used to monitor the changes of VHH_{2,4-D} coated on microplates during ELISA procedures, but no obvious reduction was observed (Fig. S1a). Then the differences in nonspecific adsorption were further examined, in which series of concentrations of wild phages were added to VHH_{2,4-D} and MBP-VHH_{2,4-D} coated wells, and higher nonspecific binding was observed in MBP-VHH_{2,4-D} coated wells (Fig. S1b). So far, the above suspicion was not supported experimentally. Therefore, we surmised that the hydrophobic regions or ionic groups for adsorption to the microplate are all close to complementarity determining regions (CDRs) because of the relatively tiny size of VHH_{2,4-D}, compared to commonly used monoclonal antibody or MBP fused VHH, it makes VHH_{2,4-D} unable to keep the advantageous spatial orientation for antigen recognition after being adsorbed so that the reactivity of coated VHH_{2,4-D} to phage display peptidomimetic was reduced. Further, it also greatly affects the recognition of VHH_{2,4-D} to 2,4-D, which resulted in a decrease of sensitivity. Whereas, the fusion of MBP with VHH_{2,4-D} expanded the regions that can be used for adsorption and moved adsorption sites away from CDRs, which was beneficial to keep the optimal orientation for antigen recognition.

To analyze the individual contribution of the peptidomimetic residues, each amino acid was mutated into alanine (A), and the twelve phage display peptidomimetic mutants were tested for their reactivities to MBP-VHH_{2,4-D} using phage ELISAs. The result showed that only two mutants (N1A, V9A), which showed similar reactivities to the original sequence (Fig. 1d). The result indicated that the binding between the peptidomimetic and VHH_{2,4-D} requires the cooperation of multiple amino acids. In previous research, it was demonstrated that 2,4-D reacts with the tunnel formed by the CDR3 and frame regions in VHH_{2,4-D} (Li et al., 2021). Because the peptidomimetic can compete with 2,4-D to bind with VHH_{2,4-D}, it is reasonable to assume that the peptidomimetic also reacts with VHH_{2,4-D} around this tunnel, and utilizes the cooperation of multiple amino acids to block the access of 2,4-D to its binding site. Considering that the peptidomimetic of aflatoxin B₁ previously reported is also 12-amino-acids peptide (Zhao et al., 2019), we think there is greater success rate for peptidomimetic acquisition from long peptide library.

3.2. Design of the “ready-to-use” immunosensor

NanoLuc binary technology (NanoBiT) is a new tool for studying molecular interactions. The Nluc was split into two inactive fragments (SmN, 1.3 kDa and LgN, 17.7 kDa) and coupled to a pair of interacting molecules respectively. The interaction between molecules would drive the reassociation of Nluc, thus significantly increases the luminescence intensity of the system (Dixon et al., 2016). Recently, NanoBiT has begun to be applied to clinical diagnosis (Zhou et al., 2021), intracellular proteins interaction (Qiao et al., 2020), and other applications.

For development of the “ready-to-use” immunosensor based on NanoBiT, SmN was fused to the N terminus of VHH_{2,4-D} to place it close to the antigen binding site of VHH, and the peptidomimetic was fused to the N terminus of LgN because SmN is located at the C terminus of LgN in native enzyme. Considering that the recombinant expression of the peptidomimetic is usually accompanied by a reduction in avidity (usually 5 copies in p β display or more copies in p γ display). This would bring the risk of the poor positive signal and S/N ratio in the recombinant peptidomimetic-based immunoassays, especially for the assays without separation or washing steps. In order to avoid this and optimize the interaction of the peptidomimetic with the VHH, we build various versions of the Pm-LgN and the SmN-VHH. To that end, the monovalent, divalent and trivalent peptidomimetics were fused with LgN with or without spacer, and a series of recombinant proteins of SmN and VHH_{2,4-D} with different spacer lengths were prepared and analyzed by SDS-PAGE gel (Fig. 2).

Theoretically, the stronger the affinity between the VHH and the peptidomimetic, the fewer unreacted reagents in the system at equilibrium, which in turn will improve the positive signal and S/N ratio. For that reason, the affinities between Pm-LgNs and Sm-VHHs were first studied. The RLUs varying with time were monitored and fitted to the reaction kinetics curve between Pm-LgNs and Sm-VHHs, which conformed to the pseudo first order reaction (Fig. S2 and S3). The k_{obs} s were calculated from the kinetics curves and linearly fitted with the concentrations of Sm-VHHs (Fig. S4). Then K_D values were obtained by the ratio of intercept (k_{off}) and slope (k_{on}) of linear equations (Table S3). The changes in the affinities between Pm-LgNs and Sm-VHHs can be clearly observed: (1) With the increase of the peptidomimetic’s valence, there is no doubt that the affinities between Pm-LgNs and Sm-VHHs have been significantly increased, the K_D values were more than ten times lower when the peptidomimetic was trimerized (Fig. 3a); (2) The spacer between the peptidomimetic and LgN caused a slight affinity increase (Fig. 3b), the K_D values of Pm-LgNs without spacer were 0.839~2.88 times that of Pm-LgNs with spacer. However, compared with the other two factors, its influence was not significant; (3) The longer spacer between SmN and VHH_{2,4-D} also reduced the affinity (Fig. 3c). The K_D values increased 3.05~5.95 times when the spacer increased from 8 amino acids to 24 amino acids. Because there was no obvious explanation for the decrease in affinity caused by longer spacer length, so the 3D models of four SmN-VHHs were predicted by RoseTTAFold (Baek et al., 2021) (Fig. 3d~j), and the models showed that SmN would be closer to the binding pocket of 2,4-D to VHH_{2,4-D} with the increase of spacer length, which may interfere the binding of the peptidomimetic and lowering the affinity of the interaction.

The binding between VHH_{2,4-D} and the peptidomimetic only is the first step for signal generation, it also requires the reassociation between LgN and SmN. Therefore, after examination of the affinities, the influence factors on positive signal of the immunosensor were subsequently studied (Table S3), which indicated that the changing regulars of positive signals were not exactly in line with their affinities. The differences were embodied in: (1) Although the spacer between peptidomimetic and LgN showed little effect on affinities, it can increase the positive signal several times (Fig. 4a). Especially for monovalent Pm-LgNs, the K_D values of Pm-LgNs with spacer were similar to (0.902~1.02 times) Pm-LgNs without spacer, but the positive values were improved 6.36~14.9 times. In addition, the K_D values of SmNVHH group were 0.448~1.12 times than the SmN-S₁-VHH, but the positive values of SmN-S₁-VHH were 1.52~4.92 times higher (Fig. 4b). So the spacers were believed to offer the favorable spatial orientations for the reassociation of Nluc after the binding between peptidomimetic and VHH_{2,4-D}, which were the essential components in the “ready-to-use” immunosensor; (2) Although the K_D values of trivalent peptidomimetics were 0.0609~0.271 times better than divalent peptidomimetics, the positive signals of divalent peptidomimetics were 1.49~3.83 times higher than trivalent peptidomimetics (Fig. 4c). We speculated that the functional peptidomimetic has a more rigid structure than the spacer formed by GGGs, when peptidomimetic expressed in series would extend the distance between LgN and SmN after binding with VHH_{2,4-D} thus reducing the positive signal of immunosensor.

The background signals of these combinations needed be considered before discussing the S/N ratio. Because there is still the weak residual binding affinity between LgN and SmN ($K_D=190 \mu\text{M}$) (Dixon et al., 2016), which means that even when the binding between the peptidomimetic and VHH was dissociated by the analyte, a small amount of Nluc also can be formed. The 2,4-D standard solution at a 50-fold higher concentration than that of Pm-LgN and Sm-VHH was added to fully dissociate the peptidomimetic-VHH_{2,4-D} complex and then the remaining RLU was measured as the background signal (Table S3). Meanwhile, the 50-fold higher concentration of 2,4-D was also added to the combinations of LgN and Sm-VHHs, and no change of RLUs was observed so that can exclude the possibility of nonspecific decrease of RLU caused by 2,4-D. Overall, the results showed that the most influential factors were the spacers: (1) The spacer between the peptidomimetic and LgN not only influence the reassociation driven by peptidomimetic and VHH_{2,4-D}, but also the background reassociation. The background signals of the Pm-LgNs with spacer were 3.19~9.10 times higher than Pm-LgNs without spacer (Fig. 4d); (2) The SmNVHH group showed the strongest background signals. Compared with SmN-S₃-VHH group that showed the weakest background signals, the spacer of 24 amino acids reduced the background signals to 5.96%~20.0% of SmNVHH group (Fig. 4e). It has been mentioned above that the longer spacer would make SmN closer to the binding site of peptidomimetic, which not only seems to interfere with the binding between the peptidomimetic and VHH_{2,4-D}, this interference also make it difficult for the binding of SmN to LgN in an optimal spatial orientation. In addition, the divalent peptidomimetics showed a slight increase in background signals, which were 1.05~1.91 times than monovalent peptidomimetics and 1.50~3.72 times than trivalent peptidomimetics (Fig. 4f). Then, the S/N ratios of these combinations showed the following changes: (1) The spacer between the peptidomimetic and VHH_{2,4-D} increased the positive signals as well as the background signals, so that

its effect on improving S/N ratio was not outstanding. The S/N ratios of Pm-LgNs with spacer were 0.388~1.72 times than Pm-LgNs without spacer (Fig. 4g); (2) SmNVHH group showed the worst S/N ratios due to the poor positive signals and highest background signals, while the S/N ratios can be increased by 1.51~6.96 times when a spacer with 8 amino acids was inserted between SmN and VHH_{2,4-D}. The S/N ratios became less affected when the length of spacer continued to be increased, while the S/N ratios of SmN-S₂-VHH and SmN-S₃-VHH were 0.959~2.08 and 0.821~1.46 times than SmN-S₁-VHH, respectively (Fig. 4h); (3) The monovalent peptidomimetics showed the worst S/N ratios, while the divalent peptidomimetics were 1.35~4.26 times higher than monovalent peptidomimetics. It is not beneficial when the peptidomimetic's valence continued to be increased (the S/N ratios of trivalent peptidomimetics were 0.451~1.15 times than divalent peptidomimetics) (Fig. 4i).

Eventually, the combination of P²-LgN + SmN-S₁-VHH showed the best positive signal. At the concentrations of 0.4 μmol L⁻¹ for P²-LgN and SmN-S₁-VHH, the positive signal was 1.597×10⁷ that was clearly visible signal to the naked eye (was showed in the smaller image inserted into Fig. 4a). The higher positive signal means fewer reagents required, so as to ensure the sensitivity of competitive immunoassay. Meanwhile, this combination also showed the attractive S/N ratio of 22.23. Besides, the combination of P²-LgN + SmN-S₂-VHH showed the best S/N ratio. Although the K_D value was 18.28 μM that was much lower than the common affinity between antigen and antibody, it achieved S/N ratio of 40.73, while the positive signal was 2.418×10⁶ at the concentrations of 0.4 μmol L⁻¹ for P²-LgN and SmN-S₂-VHH. The S/N ratios were better than the widely used homogeneous immunoassays, such as resonance energy transfer (RET) and inner-filter effect (IFE). Xue et al. (2017) had reported a semisynthetic sensor based on bioluminescent RET (BRET), in which the antibody, competitive antigen and tracers of BRET were integrated into a macromolecule. Its S/N ratio of 21.55 achieved the best of the previously reported BRET sensors. Compared to the homogeneous immunoassay also used recombinant peptidomimetic, Peltomaa et al. (2018) fused peptidomimetic with yellow fluorescent protein (YFP) and developed a fluorescent RET (FRET) immunoassay using YFP as the donor and colloidal gold as the receptor. After optimizing the diameter and dosage of colloidal gold, the fluorescence recovery rate was about 4 times. Compared to the FRET that also used VHH as the recognition antibody (Tang et al., 2020), the authors demonstrated that the utilization of VHH with its tiny size would reduce the distance between donor and receptor so that it can produce higher transfer efficiency, however, the fluorescence recovery rate of the donor was less than 2 times that when the analyte dissociated the donor and acceptor. Chen et al. (2019) prepared a tetravalent dendrimer-like peptide ligand by chemical synthesis so that greatly improved its affinity with antibody, then employed the tetravalent peptide to develop IFE immunoassay, in which the S/N ratio was less than 5 times. Generally, it is not easy to obtain a high S/N ratio in homogeneous assays (Liu et al., 2021), especially for the receptors and ligands with weak affinity. However, through the above studies, the binding between the peptidomimetic and VHH_{2,4-D} has been well adapted with the reassociation of LgN and SmN to give a luminescent product, then resulted in the “ready-to-use” immunosensor that produced a very high positive signal and S/N ratio.

3.3. Detection of 2,4-D using the “ready-to-use” immunosensor

Because the combination of P²-LgN + SmN-S₁-VHH performed well in yielding a positive signal and S/N ratio, it was used to develop the “ready-to-use” immunosensor for the detection of 2,4-D. Its principle was as follows (Fig. 5a): the binding between the peptidomimetic and VHH_{2,4-D} promoted the reassociation of the two fragments into functional Nluc so that strong bioluminescent signal was generated, with the increase of 2,4-D concentration, the binding of the peptidomimetic to VHH_{2,4-D} was gradually dissociated, then the bioluminescent signal was decreased that made the luminescence intensity negatively correlated with the concentration of 2,4-D. After 10 minutes of incubation, the reaction reached equilibrium (Fig. S5) and the luminescence intensity can be measured by the SpectraMax M5 (Molecular Devices) or visually observed using the naked eye after the addition of the Nluc substrate.

A series of molar ratios of P²-LgN and SmN-S₁-VHH in the immunosensor was tested for improved sensitivity. The molar concentration of P²-LgN or SmN-S₁-VHH was fixed at 0.2 μmol L⁻¹, and the molar concentration of the other reagent was changed by gradient. The 2,4-D concentrations and corresponding RLUs were fitted according to four parameter equation by GraphPad Prism 8. Then the IC₅₀ of different molar ratios were obtained to evaluate the sensitivities. The results showed that the increase of P²-LgN's molar concentration would improve the positive signal and the sensitivity would not be affected in a certain range (Fig. S6a), while the increase of SmN-S₁-VHH concentration also would improve the positive signal and the sensitivity would become worse at the same time (Fig. S6b). Finally, the molar ratio 0.2:0.025 μmol L⁻¹ of P²-LgN:SmN-S₁-VHH was used to develop the standard curve for the immunosensor for detection of 2,4-D (Fig. 5b). The IC₅₀, limit of detection (LOD, IC₁₀) and linear range (IC₁₀~IC₉₀) were 3.64, 0.728 and 0.728~18.2 ng mL⁻¹, respectively. Compared with other reported immunoassays for 2,4-D (Table S4), the sensitivity of the “ready-to-use” immunosensor is only slightly lower than the fluorescent immunoassay (IC₅₀ was 1.9 ng mL⁻¹) using the recombinant protein of VHH_{2,4-D} and alkaline phosphatase (Li et al., 2021), and the bioluminescence immunoassay (IC₅₀ was 2.15 ng mL⁻¹) using Nluc-labelled phage (Ding et al., 2021). For visual observation, we also optimized the molar ratios of P²-LgN and SmN-S₁-VHH to ensure the visual positive signal for naked eye and better sensitivity. The results showed that the molar ratio 0.8:0.1 μmol L⁻¹ of P²-LgN:SmN-S₁-VHH got the best sensitivity and the visible positive signal (Fig. S7), in which a significant decrease in luminescence intensity was observed when the concentration of 2,4-D reached 16 ng mL⁻¹ (Fig. 5c). Cross-reactivities (CRs) to 2,4-D's analogues were used to assess the specificities of the immunosensor. The results indicated that the immunosensor showed similar specificities to other immunoassays using the same VHH_{2,4-D} (Li et al., 2021), in which there was no obvious CRs (CR 2.58%) to the analogues except for 2-methyl-4-chloro-phenoxyacetic acid (CR=17.8%) (Table S5). We further investigated performances of the immunosensor after treatment of 60 °C and 25 °C. The result showed that the immunosensor has a low tolerance to high temperature (60 °C), in which the positive signal decreased significantly after 2 minutes and the IC₅₀ increased significantly after 5 minutes (Fig. S8a). Since unsplit Nluc shows high thermostability, the result maybe indicated that the split of Nluc decrease its thermostability. Under the incubation of reaction temperature (25 °C), the immunosensor

can maintain the positive signal and IC₅₀ within 5 hours, while the deterioration in performances occurred at 8 h incubation (Fig. S8b). In spite of the poor performances after treatment of 60 °C, we believe stability of the immunosensor is sufficient to complete the detection.

Subsequently, the immunosensor was used to detect the concentrations of 2,4-D in spiked wheat samples. Considering that the wheat matrix may affect the immunoassay, we first examined the influence of the wheat matrix on the “ready-to-use” immunosensor. Twenty microliters blank extracting solutions containing serial concentrations of 2,4-D were used to establish the matrix standard curves directly or after being diluted 2 and 3-fold. Due to the extra 2-fold dilution in extraction process and 5-fold dilution in detection process, the total dilution ratios of wheat matrix were 10, 20 and 30-fold, respectively. The results demonstrated that the standard curve run in 30-fold diluted matrix was basically consistent with the standard curve run in PBS (Fig. S9a). It was noticed that the bioluminescence signal decreased when the concentration of wheat matrix was greater than 1/30. The sample matrix usually affects the interaction between antibody and antigen. However, when the ordinates of these standard curves were converted from RLU to the inhibition ratio of 2, 4-D on RLU, the standard curves were not affected in the wheat matrix at less than 1/10 concentration (Fig. S9b). Therefore, it was speculated that the effects of wheat matrix on signal generation was greater than that on the competition of 2,4-D. Considering that the reduction of luminescence would affect the visual detection, the dilution factor was finally determined to be 30-fold.

Then the concentrations of 2,4-D in spiked samples were analyzed by the immunosensor after a 30-fold dilution. The average recoveries and relative standard deviations (RSDs) were 84.1~102.3% and 5.7~9.2%, respectively, while the results of visual observation were also consistent with the spiked concentrations (Table 1). Considering that the maximum residues limits of 2,4-D in wheat is 2 µg g⁻¹ (GB 2763-2021), the “ready-to-use” immunosensor can meet the regulatory requirement of actual detection.

4. Conclusions

In this work, we successfully developed a “ready-to-use” immunosensor with high positive signal, S/N ratio and sensitivity. This immunosensor realizes the goal of labelling-free, immobilization-free and washing-free analysis, which significantly improves the efficiencies of reagent production and detection procedures, and makes it ideal for point of care formats. In addition, the recombinant proteins reagents used in the immunosensor can be produced in large quantities by bacterial fermentation in a highly cost effective way, and one even can just store its DNA sequence information as “raw materials” for the long-term storage.

Key aspects for the development of the immunosensor were carefully studied in this work. The first aspect is peptidomimetic acquisition. In order to obtain a useful peptidomimetic, we explored six conditions, two target receptors with different relative molecular weights, and the use of three phage display libraries. We found that the recombinant expression of the VHH with appropriate carrier protein (like MBP) is conducive to maintaining its optimal spatial orientation for the capture of peptidomimetic from library, and the use

of long peptide libraries appears to help to increase the odds of a positive selection. The second aspect address in this study was the design of immunosensor for the better performances. The process of signal generation was divided into two parts: the binding between peptidomimetic and VHH_{2,4-D}, and the reassociation of LgN and SmN into the luminescent Nluc, then the roles of spacer between peptidomimetic and LgN, copy numbers of peptidomimetic and spacer between SmN and VHH_{2,4-D} were analyzed in the development of the “ready-to-use” immunosensor: (1) The spacer between peptidomimetic and LgN is the most critical factor to improve the positive signal output, while the spacer showed no obvious effect in improvement of affinities between the peptidomimetic and VHH_{2,4-D}. Unfortunately, this spacer is also leads to an increase the background signal. (2) The more copy numbers of peptidomimetic can significantly improve its affinities to VHH_{2,4-D}. However, the long peptidomimetic may contribute to pull away the SmN and LgN after binding to VHH, thus causes the reductions of the positive signal and S/N ratio. In this study, the divalent peptidomimetic in Pm-LgN turned out to be optimal. (3) The longer spacer between SmN and VHH_{2,4-D} interferes with the binding of the peptidomimetic to VHH_{2,4-D}, but it is beneficial to improve the positive signal and reduce the background signal. In this study, the spacers of 8~16 amino acids were optimal for obtaining the high positive signal and S/N ratio. After optimization, the combination of P²LgN+SmN-S₂-VHH achieved the best S/N ratio of 40.73, which was better than the homogeneous format widely used in immunoassays. In addition, the combination of P²-LgN+SmN-S₁-VHH showed the best positive signal and an attractive S/N ratio of 22.23, which generated a clearly visible signal at a concentrations of 0.4 μmol L⁻¹ for P²-LgN and SmN-S₁-VHH.

The combination of P²-LgN+SmN-S₁-VHH was used to develop the “ready-to-use” immunosensor for the detection of 2,4-D with an IC₅₀ of 3.64 ng mL⁻¹, which was higher sensitive than the ELISA using the phage display peptidomimetic and several other widely reported immunoassays for 2,4-D. In addition, this immunosensor also showed good accuracy for detection of 2,4-D in spiked samples. With a rapid turnaround time and consistent reagents, thus, we believe that the “ready-to-use” immunosensor with fast readout is a unique contribution to the toolbox for small molecule detection. However, the inadequacies of the immunosensor is the “signal-off” mode, which made the result not very straightforward, especially for visual inspection. For this consideration, the peptidomimetic can be replaced by anti-immunocomplex peptide to develop noncompetitive immunoassay so that can make detection results of the “ready-to-use” immunosensor more intuitive and friendly. Even so, we believe that the panning strategy for peptide ligands and design strategy of the immunosensor summarized in this study would be helpful to guide developments of NanoBiT-based sensors.

Supplementary Material

Refer to Web version on PubMed Central for supplementary material.

Acknowledgement

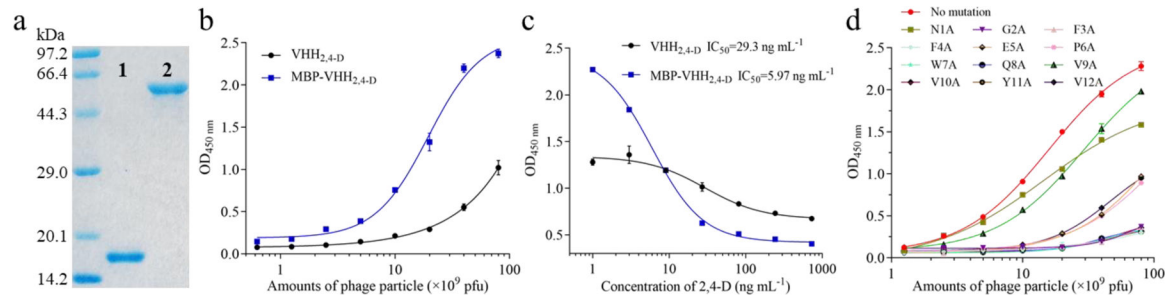
This work was supported by the National Natural Science Foundation of China (Grant 32102258 and 32172451), the Jiangsu Planned Projects for Postdoctoral Research Funds (2021K103B). Partial funding was provided by National Institute of Environmental Health Science Superfund Research Program (P42ES004699) and National

Institute of Health RIVER Award (R35 ES030443-01). Molecular graphics and analyses performed with UCSF Chimera, developed by the Resource for Biocomputing, Visualization, and Informatics at the University of California, San Francisco, with support from NIH P41-GM103311.

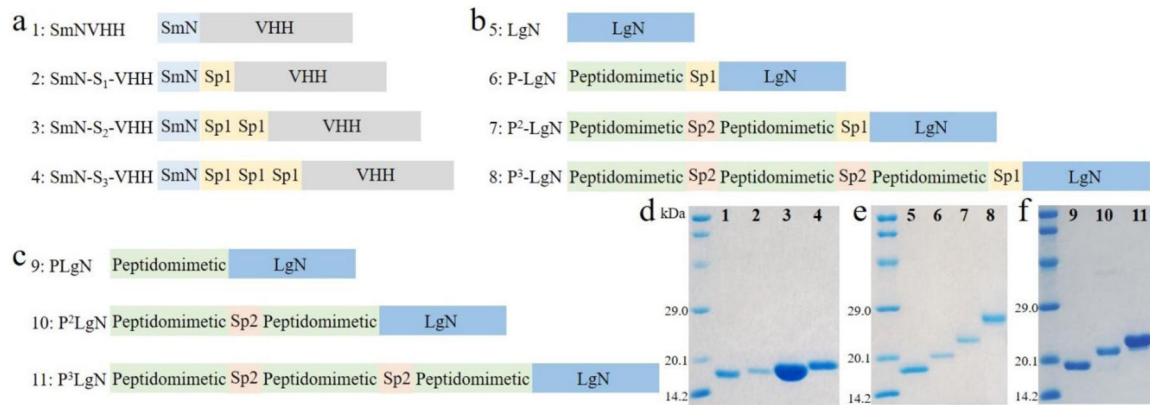
References

- Ai ZJ, Zhao M, Han DB, Chen K, Xiong DM, Tang H, 2021. *Biosens. Bioelectron* 179, 113059. 10.1016/j.bios.2021.113059 [PubMed: 33561664]
- Adamson H, Jeuken LJC, 2020. *ACS Sens* 5, 3001–3012. 10.1021/acssensors.0c01831 [PubMed: 33052043]
- Baek M, DiMaio F, Anishchenko I, Dauparas J, Ovchinnikov S, Lee GR, Wang J, Cong Q, Kinch LN, Schaeffer RD, Millan C, Park H, Adams C, Glassman CR, DeGiovanni A, Pereira JH, Rodrigues AV, van Dijk AA, Ebrecht AC, Opperman DJ, Sagmeister T, Buhlheller C, Pavkov-Keller T, Rathinaswamy MK, Dalwadi U, Yip CK, Burke JE, Garcia KC, Grishin NV, Adams PD, Read RJ, Baker D, 2021. *Science* 373, 871–+. 10.1126/science.abj8754 [PubMed: 34282049]
- Chen H, Ding Y, Yang Q, Barnych B, Gonzalez-Sapienza G, Hammock BD, Wang MH, Hua XD, 2019. *ACS Appl. Mater. Interfaces* 11, 33380–33389. 10.1021/acsmi.9b13111 [PubMed: 31433617]
- Ding Y, Chen H, Li J, Huang LR, Song GY; Li ZF, Hua XD, Gonzalez-Sapienza G, Hammock BD, Wang MH, 2021. *Anal. Chem* 93, 11800–11808. 10.1021/acs.analchem.1c02322 [PubMed: 34415158]
- Ding Y, Hua XD, Chen H, Liu FQ, Gonzalez-Sapien G, Wang MH, 2018. *Anal. Chem* 90, 2230–2237. 10.1021/acs.analchem.7b04601 [PubMed: 29280616]
- Dixon AS, Schwinn MK, Hall MP, Zimmerman K, Otto P, Lubben TH, Butler BL, Binkowski BF, Machleidt T, Kirkland TA, Wood MG, Eggers CT, Encell LP, Wood KV, 2016. *ACS Chem. Biol* 11, 400–408. 10.1021/acscchembio.5b00753 [PubMed: 26569370]
- Fang L, Liao XF, Jia BY, Shi LC, Kang LZ, Zhou LD, Kong WJ, 2020. *Biosens. Bioelectron* 164, 112255. 10.1016/j.bios.2020.112255 [PubMed: 32479338]
- Kang D, Lee S, Shin H, Pyun J, Lee J, 2020. *Biosens. Bioelectron* 150, 111921. 10.1016/j.bios.2019.111921 [PubMed: 31818754]
- Luque-Uria A, Peltomaa R, Nevanen TK, Arola HO, Iljin K, Benito-Pena E, Moreno-Bondi MC, 2021. *Anal. Chem* 93, 10358–10364. 10.1021/acs.analchem.1c02109 [PubMed: 34259504]
- Liu MM, Li L, Jin D, Liu YZ, 2021. *Nanomed. Nanobi* 13, e1697. 10.1002/wnan.1697
- Li ZF, Dong JX, Vasylieva N, Cui YL, Wan DB, Hua XD, Huo JQ, Yang DC, Gee SJ, Hammock BD, 2021. *Sci. Total. Environ* 753, 141950. 10.1016/j.scitotenv.2020.141950 [PubMed: 32906044]
- Liu XY, Wu WJ, Cui DX, Chen XY, Li WW, 2021. *Adv. Mater* 33, 2004734. 10.1002/adma.202004734
- Peltomaa R, Farka Z, Mickert MJ, Brandmeier JC, Pastucha M, Hlavacek A, Martinez-Orts M, Canales A, Skladal P, Benito-Pena E, Moreno-Bondi MC, Gorris HH, 2020. *Biosens. Bioelectron* 170, 112683. 10.1016/j.bios.2020.112683 [PubMed: 33069054]
- Peltomaa R, Amaro-Torres F, Carrasco S, Orellana G, Benito-Peña E, Moreno-Bondi MC, 2018. *ACS Nano* 12, 11333–11342. 10.1021/acsnano.8b06094 [PubMed: 30481972]
- Petterson EF, Goddard TD, Huang CC, Couch GS, Greenblatt DM, Meng EC, Ferrin TE, 2004. *J. Comput. Chem* 25, 1605–1612. 10.1002/jcc.20084 [PubMed: 15264254]
- Qiao AN, Han S, Li XM, Li ZX, Zhao PS, Dai AT, Chang R, Tai LH, Tan QX, Chu XJ, Ma LM, Thorsen TS, Reedtz-Runge S, Yang DH, Wang MW, Sexton PM, Wootten D, Sun F, Zhao Q, Wu BL, 2020. *Science* 367, 1346–+. 10.1126/science.aaz5346 [PubMed: 32193322]
- Tang ZW, Liu X, Su BC, Chen Q, Cao HM, Yun YH, Xu Y, Hammock BD, 2020. *J. Hazard. Mater* 2020, 387, 121678. 10.1016/j.jhazmat.2019.121678 [PubMed: 31753666]
- Takkinen K, Zvirbliene A, 2019. *Curr. Opin. Biotech* 55, 16–22. 10.1016/j.copbio.2018.07.003 [PubMed: 30075375]
- Vanrell L, Gonzalez-Techera A, Hammock BD, Gonzalez-Sapienza G, 2013. *Anal. Chem* 85, 1177–1182. 10.1021/ac3031114 [PubMed: 23214940]

- Wu YH, Zhou YF, Leng YK, Lai WH, Huang XL, Xiong YH, 2020. *Biosens. Bioelectron* 157, 112168. 10.1016/j.bios.2020.112168 [PubMed: 32250938]
- Wang X, Cohen L, Wang J, Walt DR, 2018. *J. Am. Chem. Soc* 140, 18132–18139. 10.1021/jacs.8b11185 [PubMed: 30495929]
- Xue L, Yu QLY, Griss R, Schena A, Johnsson K, 2017. *Angew. Chem. Int. Edit* 56, 7112–7116. 10.1002/anie.201702403
- Yao JJ, Wang ZX, Guo LL Xu XX, Liu LQ, Xu LG, Song SS, Xu CL, Kuang H, 2020. *Trac-Trend. Anal. Chem* 131, 116022. 10.1016/j.trac.2020.116022
- Zhao FC, Shi RR, Liu RX, Tian Y, Yang ZY, 2021. *Food Chem* 339, 128084. 10.1016/j.foodchem.2020.128084 [PubMed: 33152875]
- Zhou LL, Zhang LL, Yang L, Ni W, Li Y, Wu YH, 2021. *Biosens. Bioelectron* 173, 112824. 10.1016/j.bios.2020.112824 [PubMed: 33229132]
- Zhao FC, Tian Y, Shen Q, Liu RX, Shi RR, Wang HM, Yang ZY, 2019. *Talanta* 195, 55–61. 10.1016/j.talanta.2018.11.013 [PubMed: 30625581]

**Fig. 1.**

Characters of target receptors and acquired phage display peptidomimetic. (a) The SDS-PAGE gel analysis for VHH_{2,4-D} (lane 1) and MBP-VHH_{2,4-D} (lane 2); (b) The reactivities of the phage display peptidomimetic to VHH_{2,4-D} and MBP-VHH_{2,4-D}; (c) The sensitivities of the phage display peptidomimetic for the detection of 2,4-D using VHH_{2,4-D} and MBP-VHH_{2,4-D} as target receptors, respectively; (d) The reactivities of phage display peptidomimetic mutants using MBP-VHH_{2,4-D} as the target receptor.

**Fig. 2.**

Structural schematic diagrams and SDS-PAGE gel analysis of Sm-VHHs and Pm-LgNs.

The structural schematic diagrams of four kinds of Sm-VHHs (a), LgN and three kinds of Pm-LgNs with spacer (b) and three kinds of Pm-LgNs without spacer (c), in which the Sp1 and Sp2 represent the sequences of GGGSGGGS and GGGGS, respectively. The SDS-PAGE gel analysis of four kinds of Sm-VHHs (d), LgN and three kinds of Pm-LgNs with spacer (e) and three kinds of Pm-LgNs without spacer (f). The lane numbers in (d)~(f) correspond to the numbers listed in (a)~(c).

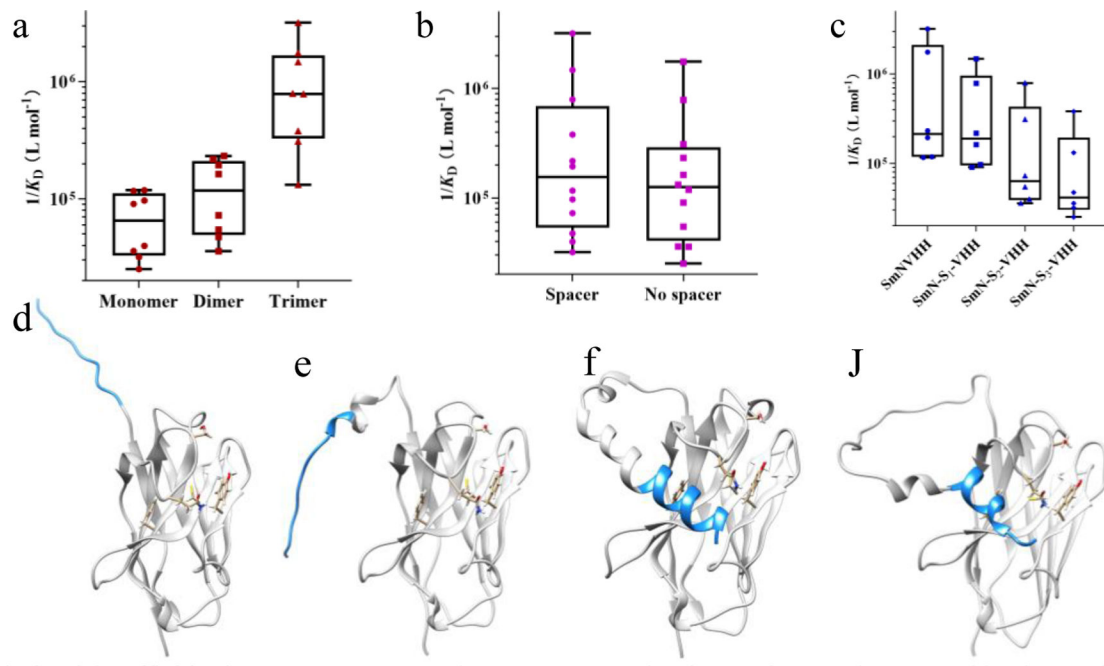


Fig. 3. Analysis of the affinities between Pm-LgNs and Sm-VHHs. (a) The changes in K_D values caused by the peptidomimetic's valences in Pm-LgNs; (b) The changes in K_D values caused by the spacer between the peptidomimetic and LgN; (c) The changes in K_D values caused by the spacer lengths between SmN and VHH_{2,4-D}; The predicted structural models of SmNVHH (d), SmN-S₁-VHH (e), SmN-S₂-VHH (f) and SmN-S₃-VHH (j), in which the displayed residues are the sites of VHH_{2,4-D} that interacted with 2,4-D, and the blue parts represent the sequence of SmN. Structure representation was performed using Chimera (Pettersen et al., 2004).

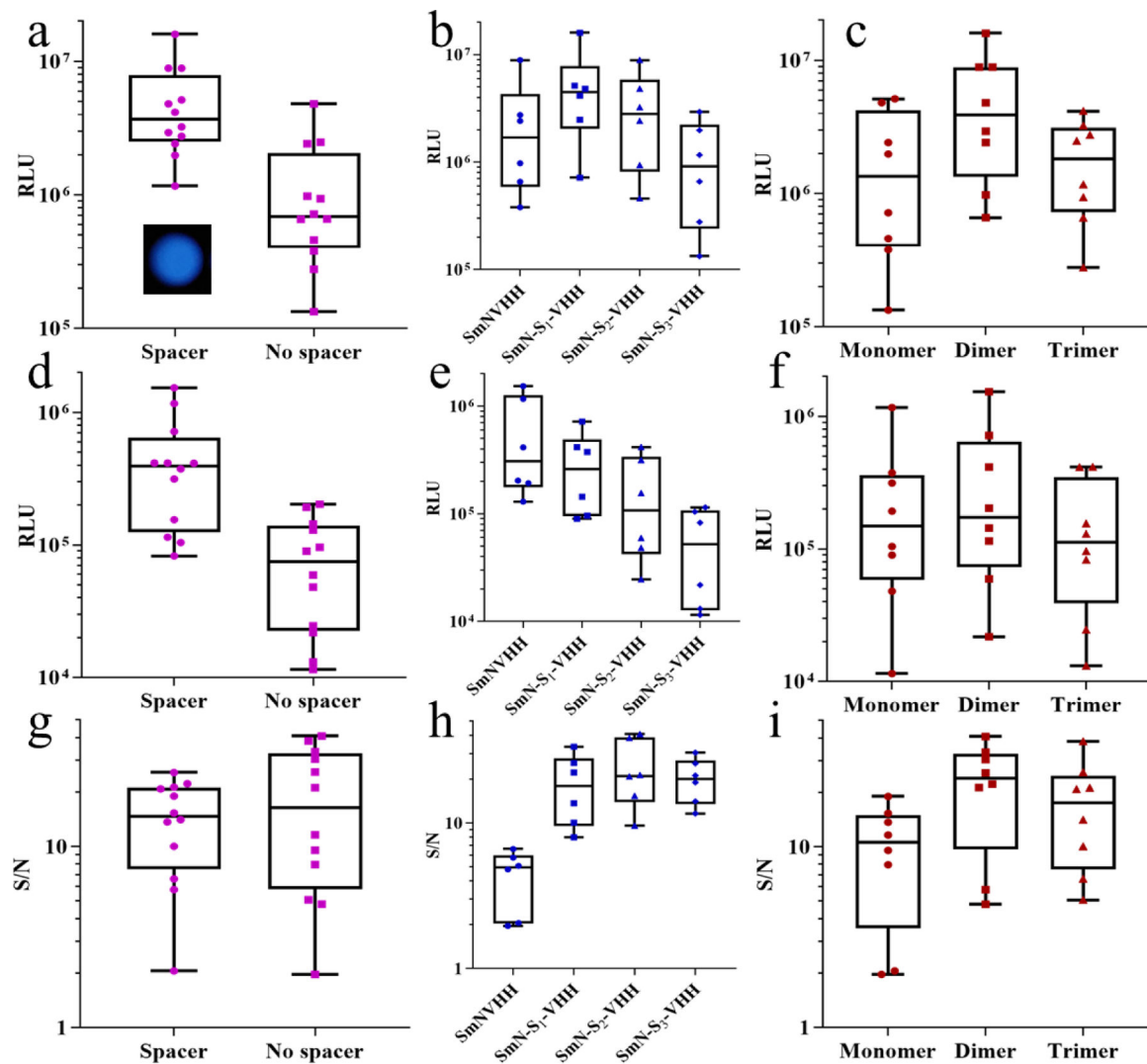


Fig. 4. Analysis of the positive signals, background signals and S/N ratios of the immunosensors. The changes in positive signals caused by the spacer between the peptidomimetic and LgN (a), the spacer lengths between SmN and VHH_{2,4-D} (b) and the peptidomimetic's valences in Pm-LgNs (c); The changes in background signals caused by the spacer between the peptidomimetic and LgN (d), the spacer lengths between SmN and VHH_{2,4-D} (e) and the peptidomimetic's valence in Pm-LgNs (f); The changes in S/N ratios caused by the spacer between the peptidomimetic and LgN (g), the spacer lengths between SmN and VHH_{2,4-D} (h) and the peptidomimetic's valence in Pm-LgNs (i).

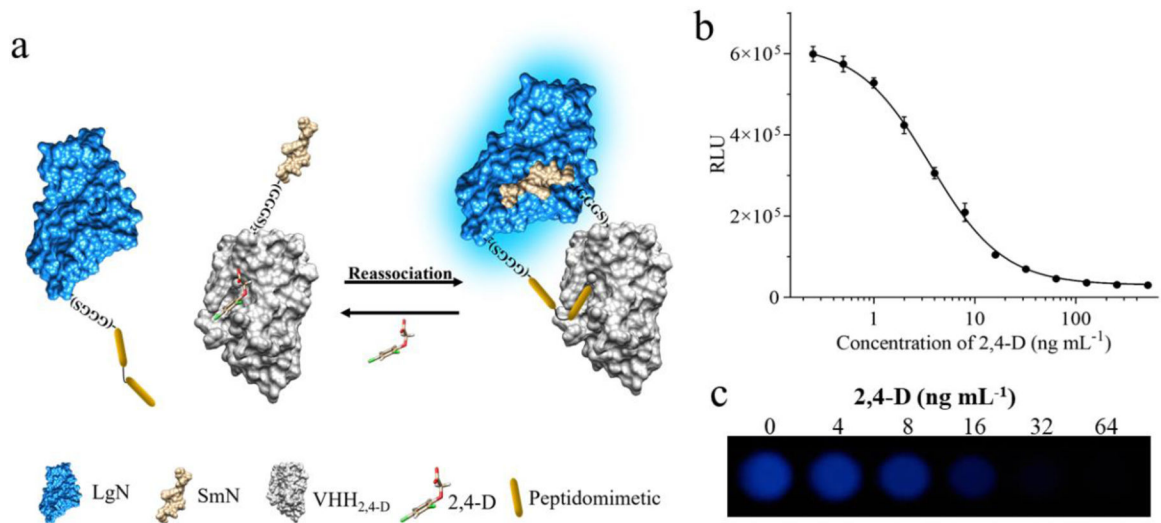


Fig. 5. Detection of 2,4-D by the immunosensor based on the combination of P²-LgN + SmN-S₁-VHH. (a) Schematic diagram of the immunosensor detection principle; (b) Standard curve for the detection of 2,4-D developed by the RLUs measured by SpectraMax M5; (c) The luminescent image under the optimal concentrations of P²-LgN + SmN-S₁-VHH.

Table 1

Detection results of spiked wheat samples by “ready-to-use” immunosensor ($n=3$).

Sample	Spiked concentration (ng g ⁻¹)	Recovery \pm SD (%)	RSD (%)	Visual observation
	0	---	---	
	40	84.1 \pm 4.78	5.7	
Wheat	160	102.3 \pm 7.20	7.0	
	640	93.5 \pm 8.56	9.2	
	1280	92.1 \pm 6.04	6.6	